International Journal of Material Forming (2023) 16:18
https://doi.org/10.1007/s12289-023-01740-9

DEVELOPMENTS IN MODELLING AND SIMULATION..JAPAN, SOUTH KOREA AND CHINA

Optimization of hot gas pressure forming process for titanium alloy component

Bao Qu[1,2] · Ling Wang[3] · Kehuan Wang[1,2] · Hongzhi Xie[3] · Jing Wei[1,2] · Jie Zhao[1,2] · Gang Liu[1,2]

Received: 26 August 2022 / Accepted: 19 January 2023 / Published online: 28 January 2023

Abstract
In this paper, hot gas pressure forming (HGPF) of titanium alloy irregularly profiled tubular component using laser-welded tube was studied by both simulation and experiment. Uniaxial tensile tests of base metal (BM) under different conditions were performed to determine the true stress–strain curves. The forming process was optimized by finite element simulation and response surface method (RSM). Results show that the forming pressure increases with the decreasing temperature and increasing strain rate. Microstructures of BM are sensitive of forming temperature, strain and strain rate. Wrinkling and local thinning of the component can be avoided by a reasonable initial tube diameter during the forming. Ideal weld position should be determined to avoid the failure of the weld seam (WS). A qualified TC2 titanium alloy component with both high dimensional accuracy and good post-form properties was successfully formed by HGPF using the optimized forming parameters. The total heating and forming time of the tube was less than 30 min. Both of the post-form properties and microstructures of the component were almost the same with the initial material.

Keywords Titanium alloy · Microstructure and properties · Response surface method · Finite element analysis · Hot gas pressure forming

Introduction

Thin-walled tubular components with irregular profiles made of titanium alloys not only have excellent properties, but also demonstrate the structure advantage of saving materials and reducing weight. However, titanium alloy has high deformation resistance, poor plasticity and large springback during room temperature forming [1, 2]. Therefore, hot forming processes have been developed: such as hot pressing (HP) [3] and superplastic forming (SPF) [4, 5]. The conventional HP and SPF processes have shortcomings of low efficiency, high cost and deteriorating properties [3, 6]. It is also very difficult to form thin-walled tubular components by conventional HP and SPF processes.

To improve the manufacturing efficiency and ensure the post-form properties, the HGPF process for integral forming of titanium alloy component was developed based on tube hydroforming process [7], which has a lower forming temperature but a higher forming speed than SPF. However, the forming condition of HGPF also brings some new challenges for titanium alloys because of the relatively high strength. Reasonable process parameters such as pressure value and forming temperature are the key to fabricate complex-shaped titanium alloys components by HGPF. At present, the researches mainly focus on the effect of process parameters on the thinning rate, defect control [8, 9] and forming limit [10, 11]. The pressure loading path affects the corner radius of varying diameter tube. The corner radii change linearly over time at the pressurization stage but exponentially over time at the constant pressure stage [12]. The average thinning ratio of the bulging area could be reduced significantly and the thickness distribution of the workpiece was more uniform with increasing of the axial feeding [13, 14]. In

✉ Kehuan Wang
kehuanhit@163.com

1 National Key Laboratory for Precision Hot Processing of Metals, Harbin Institute of Technology, Harbin 150001, China

2 Institute of High Pressure Fluid Forming, Harbin Institute of Technology, Harbin 150001, China

3 Engineering Technology Center, Shenyang Aircraft Corporation, Shenyang 110850, China

addition, Liu et al. [15] studied the non-isothermal HGPF forming of TA18 titanium alloy parts with large section difference. Paul et al. [16] performed a forming test of grade 2 titanium exhaust component, and the dimensional deviations between the formed part and the CAD reference range from -0.07 mm to 0.11 mm. At present, the method used to determine the process window are calculating the minimum bulging pressure and simulation in the HGPF [7, 17], which requires a lot of forming experiments [9, 18]. However, the process window determined by this method may be not the best one. Therefore, it is of great significance to consider the influence of process parameters on dimensional accuracy and thickness uniformity when determining the process window of HGPF. Response surface method (RSM) originally introduced by Box and Wilson [19], which was widely used in metal forming to predict the output response variables such as binder force, fillet radius of punch, friction coefficient and so on [20, 21]. However, the optimization of the process window of HGPF by RSM method has seldom been reported. What's more, the titanium alloys reported in the study of HGPF include Ti-3Al-2.5 V alloy [5], Ti-22Al-24Nb-0.5Mo alloy [22], Ti-55 alloy [23], TA15 titanium alloy [24] and CP-Ti alloy [25]. However, the HGPF of TC2 titanium alloy has seldom been reported. Therefore, it is necessary to develop an optimization method to determine the best process window for HGPF of TC2 titanium alloy component.

In this paper, a new method for determining the process window for HGPF is proposed. Different from traditional methods, this method could optimize process parameters by considering dimensional accuracy and thickness uniformity simultaneously. The uniaxial tensile behavior and microstructure evolution of TC2 titanium alloy at high temperature under different conditions were studied. Then, the forming process was optimized by finite element analysis and RSM. In addition, the selection of weld position was also analyzed. Finally, a TC2 titanium alloy tubular component with irregular profiles was formed to verify the process window. Combining with the characterization of properties and microstructure evolution, the best process window for HGPF of titanium alloys could be obtained to ensure dimensional accuracy, thickness uniformity and post-form properties of the formed part efficiently.

Materials and methods

Materials

The as-received material was a TC2 titanium alloy (Ti-4Al-1.5Mn) sheet and the average thickness is 1.8 mm. Figure 1a shows the XRD pattern of the initial sheet. As can be seen from the peak value, the original sheet is composed of α and β phases. The initial microstructure is shown in Fig. 1b. The dark phase is the β phase, and the bright phase is the α phase. The β phase are mainly distributed in the grain boundaries, and minority are in α grains. Both of the average size and volume fraction of the β phase are much smaller than those of the α phase. The TC2 titanium alloy sheet was cut according to the designed size, and then it was rolled into a tube at 650 °C, next welded by LBW. The laser power and the welding speed were 1.2 kW and 1.2 m/min, respectively.

Figure 2a is the microstructure of TC2 titanium alloy after laser welding. There are three regions: the base metal (BM), the fusion zone (FZ) and heat-affected zone (HAZ). Figure 2b shows the microstructure in FZ, which consists of coarse columnar grains with fine α′ martensitic structure in the matrix. The microstructure of HAZ contains a

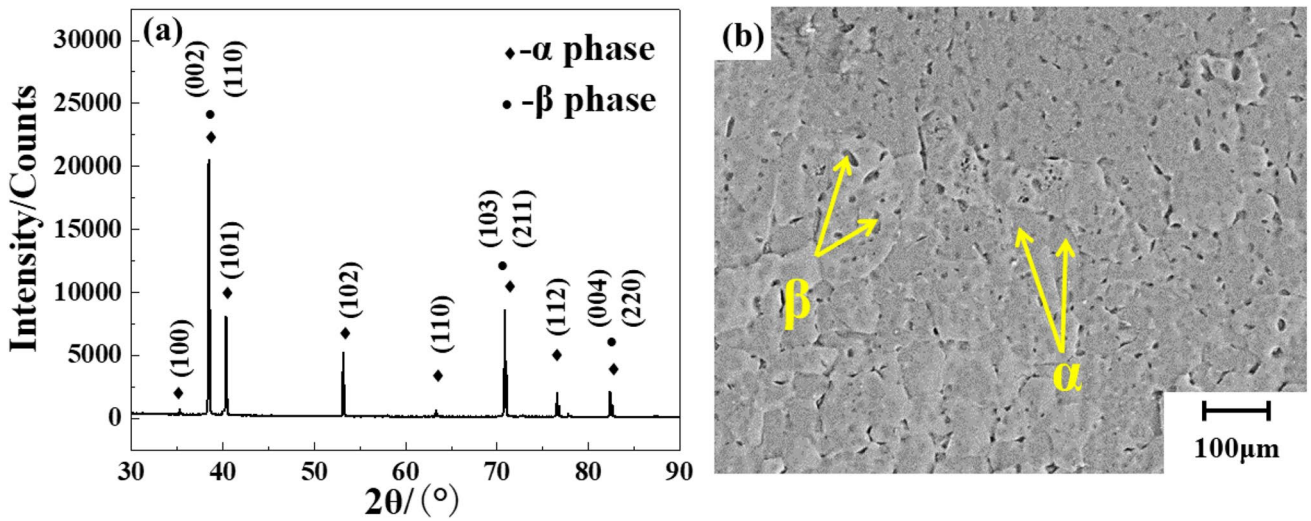

Fig. 1 XRD pattern and microstructure of the initial sheet. (**a**) XRD patterns of the TC2 alloy; (**b**) initial microstructure of the TC2 alloy sheet

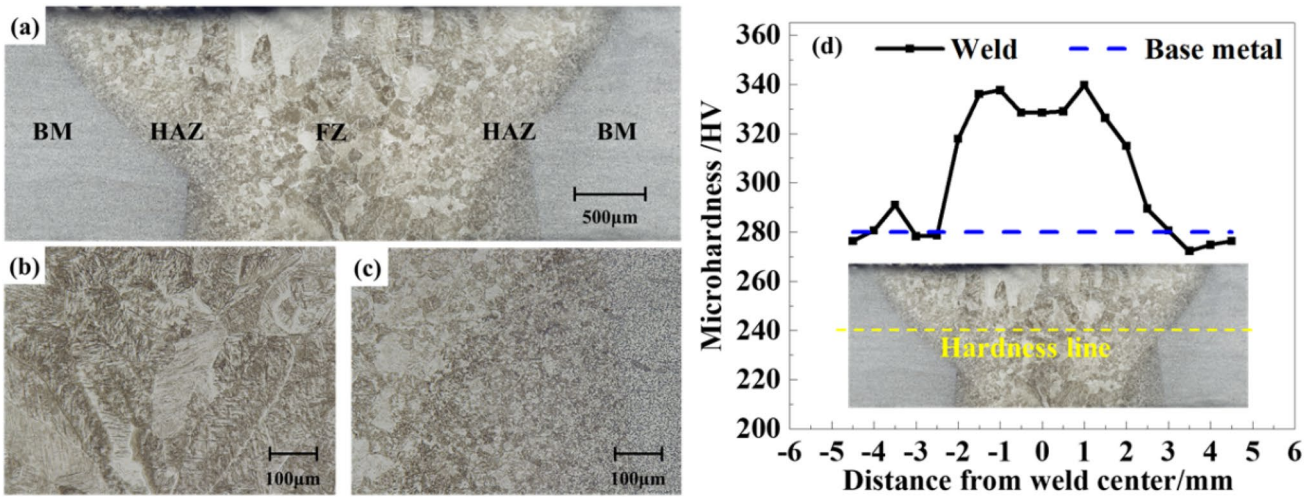

Fig. 2 Weld microstructure and microhardness. (**a**) Microstructure of LBW joint; (**b**) Microstructure of the FZ; (**c**) Microstructure of the HAZ; (**d**) Distribution of Vickers microhardness

mixture of α′, primary α phase, β phase and transformed β phase, as shown in Fig. 2c. A Vickers microhardness test machine was used to measure the hardness with a load of 0.5 kg and duration of 15 s. The microhardness is shown in Fig. 2d. It can be seen that the hardness values in the weld center zone are 328.5 ~ 339.7 HV. The hardness values in the HAZ and BM are 291.1 ~ 328.5 HV and 272.3 ~ 291.1 HV, respectively. The strength of the weld is higher than that of the base metal.

Hot uniaxial tensile and microstructure tests

Uniaxial tensile tests under different conditions were implemented to study the relationship between flow stress and strain of TC2 titanium alloy. The temperature range is from 750 to 900 °C, and strain rate range is from 0.001 to 0.1 s^{-1}. The gauge length and the width of the sample are 15 mm and 5 mm, respectively. All the tests were repeated three times. The microstructures were investigated by a Zeiss Supra55 scanning electron microscope (SEM) and optical microscope (OM). The samples were prepared by electro-polishing with a solution of 6% per-chloric acid, 34% butanol, and 60% methanol (vol %) at -40 °C with a potential of 25 V and current of 0.7 A with the time of 52 s. The polished samples were then etched using a mixture of 13% nitric acid, 7% hydrofluoric acid and 80% water (vol %) with the time of 10 s.

Finite element model of HGPF

A TC2 alloy tubular component with irregular profiles was formed. Figure 3 is the detailed dimensions of the component. The total length of component is 555.5 mm. The section length and width are about 140 mm and 52 mm, respectively. The local fillet radius is 7 mm.

The formability of the welded TC2 alloy tube is affected by process control, such as forming temperature, strain and pressurizing rate. However, the thickness accuracy of the formed part was mainly controlled by the initial tube diameter and weld position. To control the local thinning, wrinkling and flashing defects, the commercial software Abaqus was used for numerical simulation. The tube used in this paper is 555.5 mm in length, and there is no axial feeding in the HGPF process. Therefore, the tube was assumed as a plane strain state, and a 2D plane strain model as shown

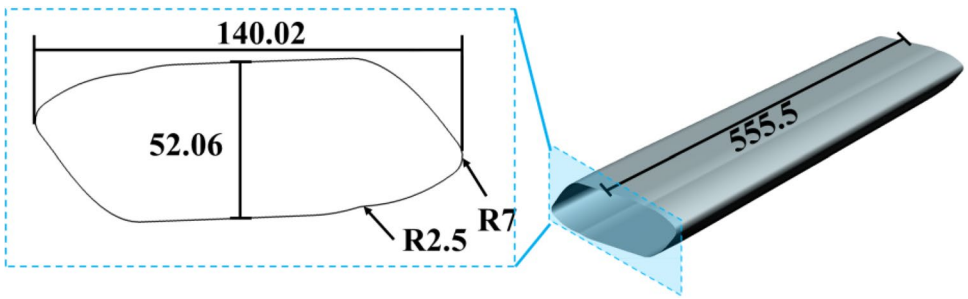

Fig. 3 The geometry of TC2 alloy component (unit: mm)

in Fig. 4 was used in the simulation. By choosing a reasonable weld position, large deformation of the weld could be avoided. In addition, the weld area occupies a very small proportion compared with the base material area. Therefore, the weld was not modeled separately during the simulation. The selection of weld position was discussed in the later section. The parameters in finite element analysis are presented in Table 1, such as analysis steps, mesh size and boundary conditions. The Mises yield criterion was adopted in this paper. True stress–strain curves of the TC2 titanium alloy obtained by hot uniaxial tensile tests were used in the simulation to describe the material flow behavior.

Hot gas pressure forming

The forming equipment and related systems are shown in Fig. 5. HGPF systems include gas pressurization system, gas pressure control system, water cooling system, heating and temperature monitoring system. In addition, it also includes forming dies, seal punches, thermocouples, gas inlet and induction coils. During the forming, the forming dies were heated to the target temperature using induction coils firstly, and then the tube was placed into the die. Three thermocouples were used to detect the temperature of the tube. The tube was heated to the target temperature after holding for 10 min, and the temperature difference of the three thermocouples was less than 5 ℃, which proved the uniformity of the tube temperature. The punches were fed to the target positions to seal the tube, and then the argon was pumped into the tube according to the specific loading route. The component was taken out of the dies and air cooled to the room temperature.

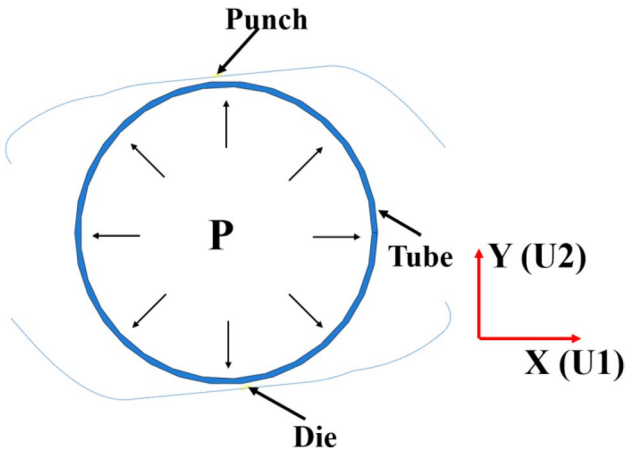

Fig. 4 Finite element model of HGPF

Results and discussion

Hot uniaxial tensile test and microstructure evolution

Hot uniaxial tensile tests under different conditions were performed to obtain the material properties. The true stress–strain curves of BM are shown in Fig. 6a-c. Since the maximum true strain of the forming part is less than 0.3, the hot uniaxial tensile test was stopped as the true strain reached 0.6 of BM. The stress increased with the decrease of temperature and the increase of strain rate. At low temperature and high strain rate, the hardening behavior is mainly caused by the increase of strain and strain rate, and the main reason of softening is necking behavior. At high temperature and low strain rate, the grain growth leads to hardening. The main reason of softening are dynamic recovery, dynamic recrystallization and phase transformation. When the temperature is higher than 750 °C, the elongation of

Table 1 Setup and parameters in finite element model

Project	2D model
Expansion ratio of initial tube size	0%, 3%, 4%, 5%, 6%
Part (die and upper)	Discrete rigid body
Tube	Deformable (Solid homogeneous)
Mesh type of die and punch	R2D2
Mesh type of tube	CPE4R
Size of mesh	0.3 mm
Tube material property	Elastic and Plastics shown in Fig. 6
	Density is 4.5E-9 kg/mm^3
Step	Dynamic explicit
Contact	Penalty contact, finite sliding and friction coefficient is 0.1
Boundary conditions	Die (U1 = U2 = UR3 = 0)
	Upper (U2 = -50 mm)
Predefined field	The temperature of the tube range is from 800 to 900 °C
Upper speed	5 mm/s

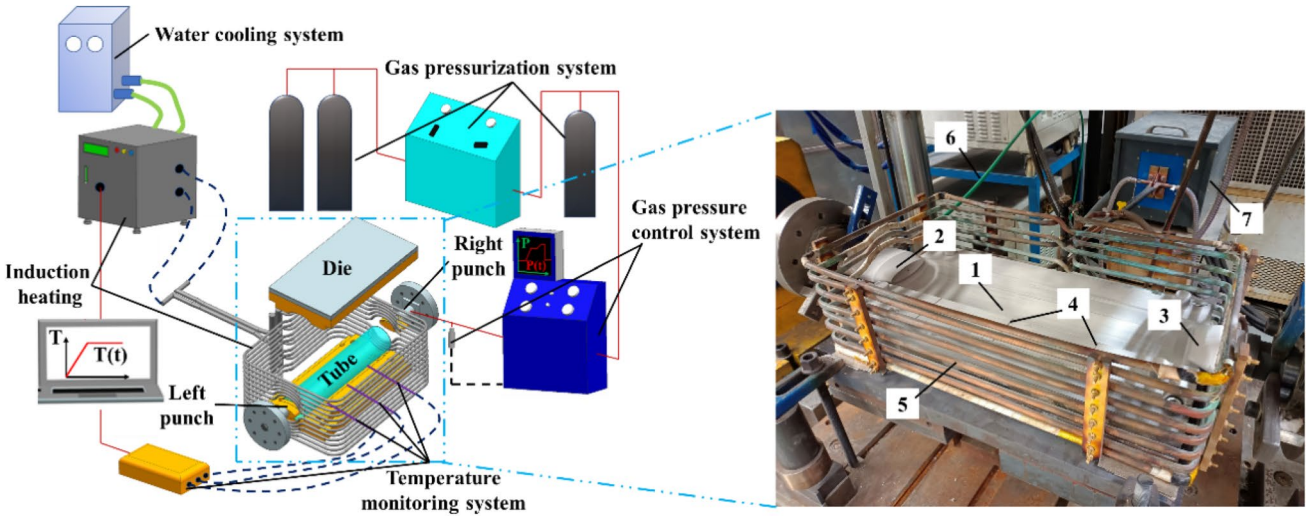

Fig. 5 Apparatuses for HGPF of TC2 alloy, where 1 is forming die, 2 is left punch, 3 is right punch, 4 is thermocouple, 5 is the induction coil, 6 is gas inlet, and 7 is heating equipment

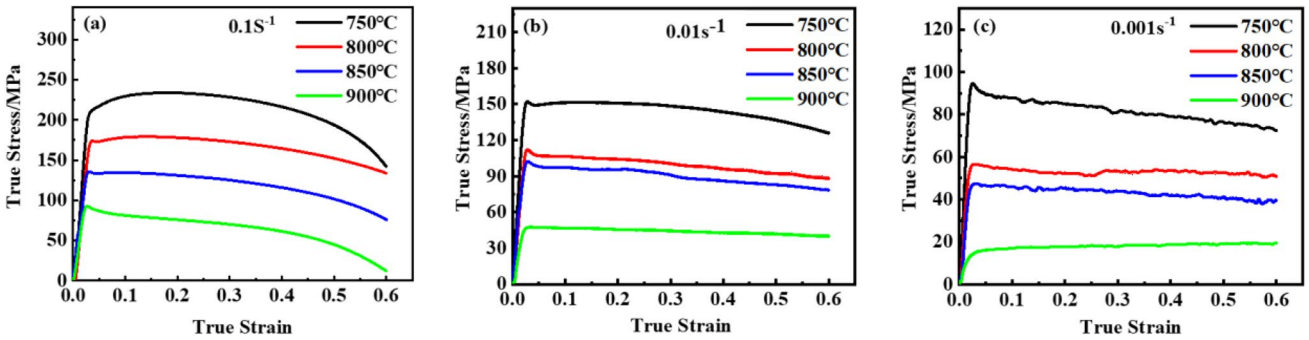

Fig. 6 True stress–strain curves of BM. (**a**) 0.1 s^{-1}; (**b**) 0.01 s^{-1}; (**c**) 0.001 $s.^{-1}$

BM is higher than 0.6, which has a sufficient elongation for HGPF. During the process of HGPF, the gas pressure required to form the minimum corner of components is the largest, which is calculated according to the formula in the reference [17]. At 800 °C/0.001 s^{-1}, the forming pressure is 15 MPa. As the 800 °C/0.01 s^{-1}, the forming pressure is higher than 30 MPa. Efficiency can be improved via a high strain rate, but the requirements for equipment also increase.

Figure 7 is the microstructures of TC2 titanium alloy after hot uniaxial tensile tests. When the strain rate is 0.01 s^{-1}, the grain size increased first and then decreased with the temperature from 800 to 900 °C as shown in Fig. 7a~c. This is because dynamic recrystallization (DRX) occurred. When the temperature is 850 °C, the grain size decreased with strain rate from 0.001 to 0.1 s^{-1} as shown in Fig. 7d~f. The grain size growth due to prolonged high temperature. Voids appeared at 850 °C/0.1 s^{-1}. The secondary α phase precipitated at 900 °C, which leads to high strength but reduced plasticity. The grain size decreased with the increasing strain due to the occurrence of DRX as shown in Fig. 7g~i. It can be seen that DRX and phase transformation are the two main factors altering the microstructure evolution. In order to maintain the initial microstructure of the material after forming, the forming temperature should be controlled at 800–850 °C.

Determination of the initial tube diameter

To determine the reasonable initial tube diameter, the finite element analysis was carried out for the initial tube with expansion ratio of 0%, 3%, 4%, 5% and 6%, respectively. When the expansion ratio of the tube is 0%, as shown in Fig. 8a. The tube collapsed seriously during die closing, and there are dead wrinkles in the HGPF because the material has no flow space. A similar risk exists for tube with a 3% expansion ratio as shown in Fig. 8b. Therefore, in the die closing process, a tube with expansion ratio of 4 ~ 6% is recommended. To further determine the expansion ratio of

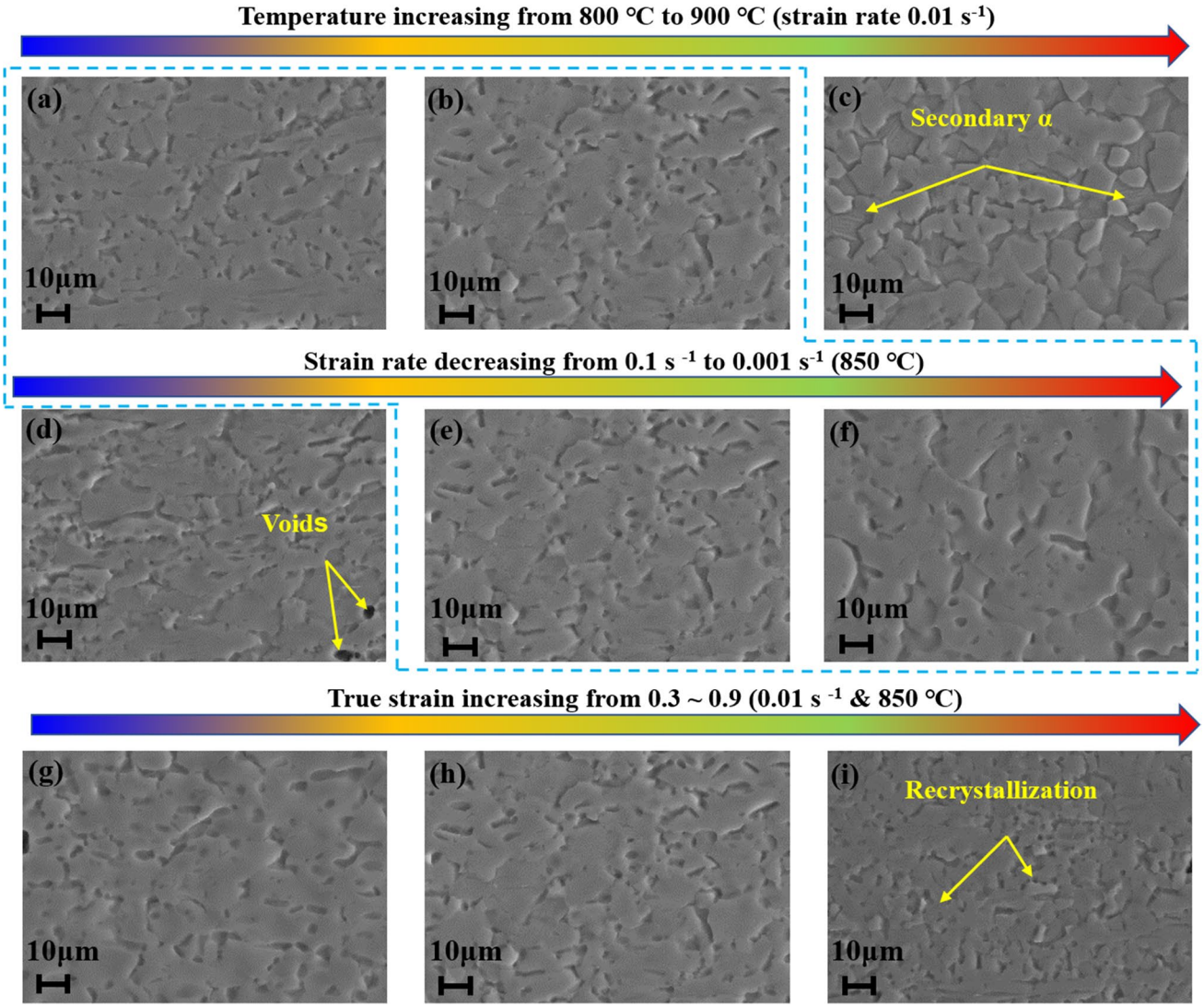

Fig. 7 SEM of the BM samples after tensile deformation, different temperature (**a**)-(**c**), different strain rate (**d**)-(**f**), different true strain (**g**)-(**i**)

the initial tube, the prediction of the thickness of the component with different expansion ratios will be discussed later.

The thinning rate increased with the increase of expansion ratio. The thickness distribution of different expansion ratios is shown in Fig. 9. The measuring points of thickness are shown in Fig. 9a. The 28 points were evenly selected along the perimeter. The minimum thickness of the component with different expansion rates is shown in Fig. 9b. Although the thinning rate of the tube with an expansion ratio of 3% is the minimum, it is prone to serious defects of wrinkling and flashing. The thickness is reduced seriously with an expansion ratio of 6%. The maximum thinning rate reached 16.11%. Therefore, it is recommended to use an initial tube with an expansion ratio between 4 and 5%. When the expansion ratio was 5%, the minimum thickness was 1.562 mm and the maximum thinning rate was 13.22%, which has met demand. Therefore, initial tube with an expansion ratio of 5% was used in this paper. The experimental result of the component with 5% expansion ratio was provided in Fig. 9c. In the preforming process (die closing), thanks to the small increase in perimeter, the thickness was distributed uniformly. In the HGPF process, the two corners were thinned due to large expansion according to Fig. 8d.

Optimization of HGPF process window

To further obtain the reasonable forming process window, including forming temperature and gas pressure, optimization was performed by the combination of finite element analysis and RSM. During the optimization, the temperature ranged from 800 to 900 ℃ and the gas pressure ranged from 5 to 20 MPa. The tube was soaked for 10 min in the

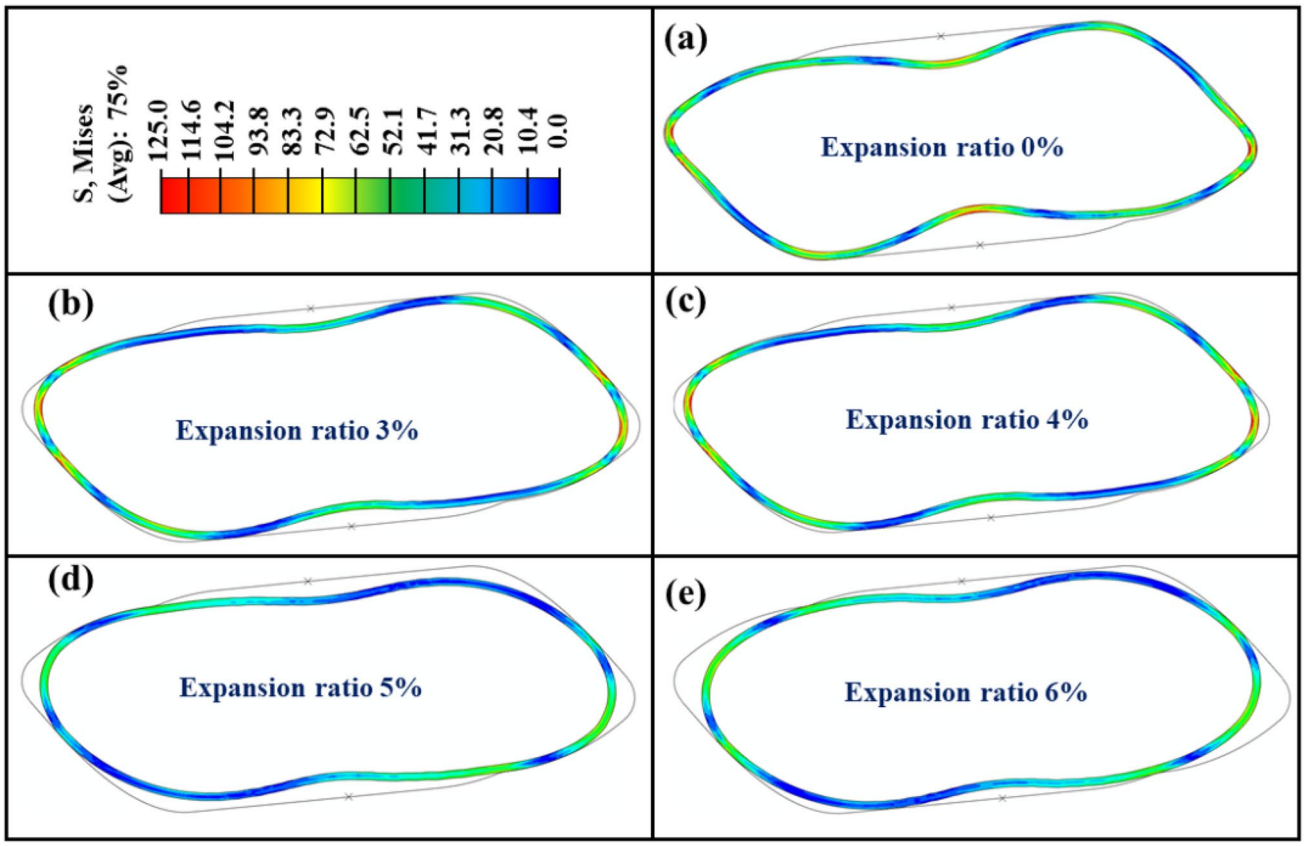

Fig. 8 Simulation results of tube with different expansion ratio. (**a**) 0%; (**b**) 3%; (**c**) 4%; (**d**) 5%; (**e**) 6%

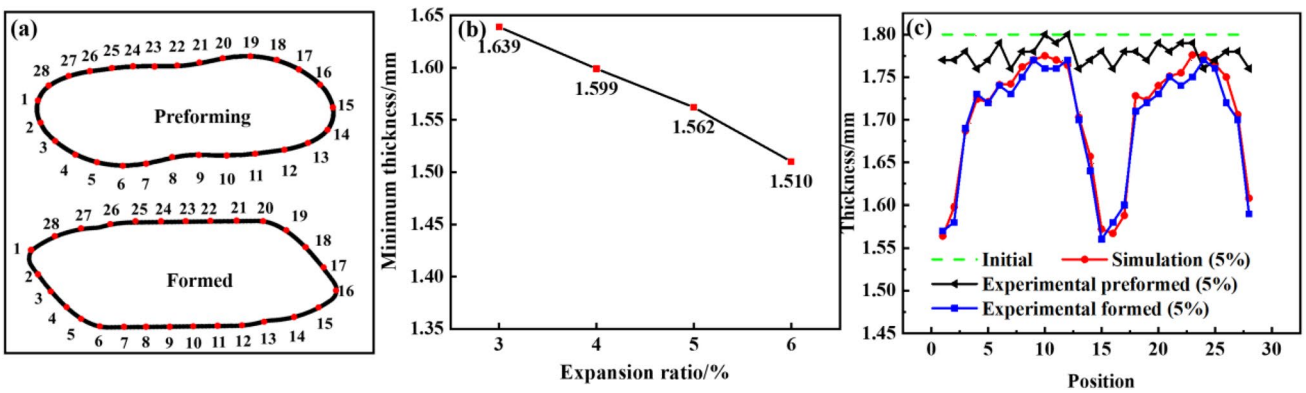

Fig. 9 Effect of expansion ratio on thickness distribution. (**a**) measuring points; (**b**) minimum thickness with different expansion ratio; (**c**) thickness distribution

heated dies before forming to stabilize the temperature, and the temperature was also constant during the forming. Therefore, the temperature was treated as a constant during the RSM. The forming process included four stages such as die closing, pressurization, forming and calibration (Fig. 13). During the calibration stage, the pressure value was the maximal one, which was also the dominant factor affecting the dimensional accuracy. Therefore, only the maximum gas pressure value in the calibration stage was optimized, and it was also treated as a constant during each simulation. To express the thickness distribution of the component more intuitively, the inhomogeneity of thickness Y is defined, which can be calculated by Eq. (1):

$$Y = 100\% \times \left(T_{max} - T_{min}\right)/T_0 \tag{1}$$

where T_{max} and T_{min} are the maximum and minimum thickness, respectively. T_0 is the thickness of initial sheet. A parameter related to dimensional accuracy *Dist* is defined, which is equal to the average distance between the corresponding points of the source point cloud and the target point cloud. The flow chart of process window optimization is shown in Fig. 10.

The Central Composite module in response surface analysis software was used to optimize the process parameters. The forming quality evaluation index Z value is defined, which is the function of inhomogeneity of thickness Y and dimensional accuracy deviation *Dist*. The Z value is an evaluation index of the degree of deviation, and the smaller the value of Z, the better the quality of the formed component. The calculation formula is shown in Eq. (2).

$$Z = 0.8 \times Dist + 0.2 \times Y/100 \tag{2}$$

The Z values were calculated via Design Expert 10.0 commercial software, and the response model after data analysis was shown in Eq. (3).

$$Z = 1.316^{-5}T^2 + 1.379^{-4}P^2 + 1.712^{-5}TP - 0.023T - 0.021P + 10.223 \tag{3}$$

where T and P are the forming temperature and gas pressure, respectively. Through regression analysis of the equation, the prediction result of response surface analysis is shown in Fig. 11. The Z value decreased first and then increased with the increasing temperature. This is because when the forming temperature was relatively low, the corner area of the component could not be fully formed due to the requirement of very high forming pressure. However, when the temperature was relatively high, the strength of forming dies decreased and the deformation of the forming dies increased accordingly, which may lead to the increase of the dimensional accuracy deviation. The Z value decreased with the

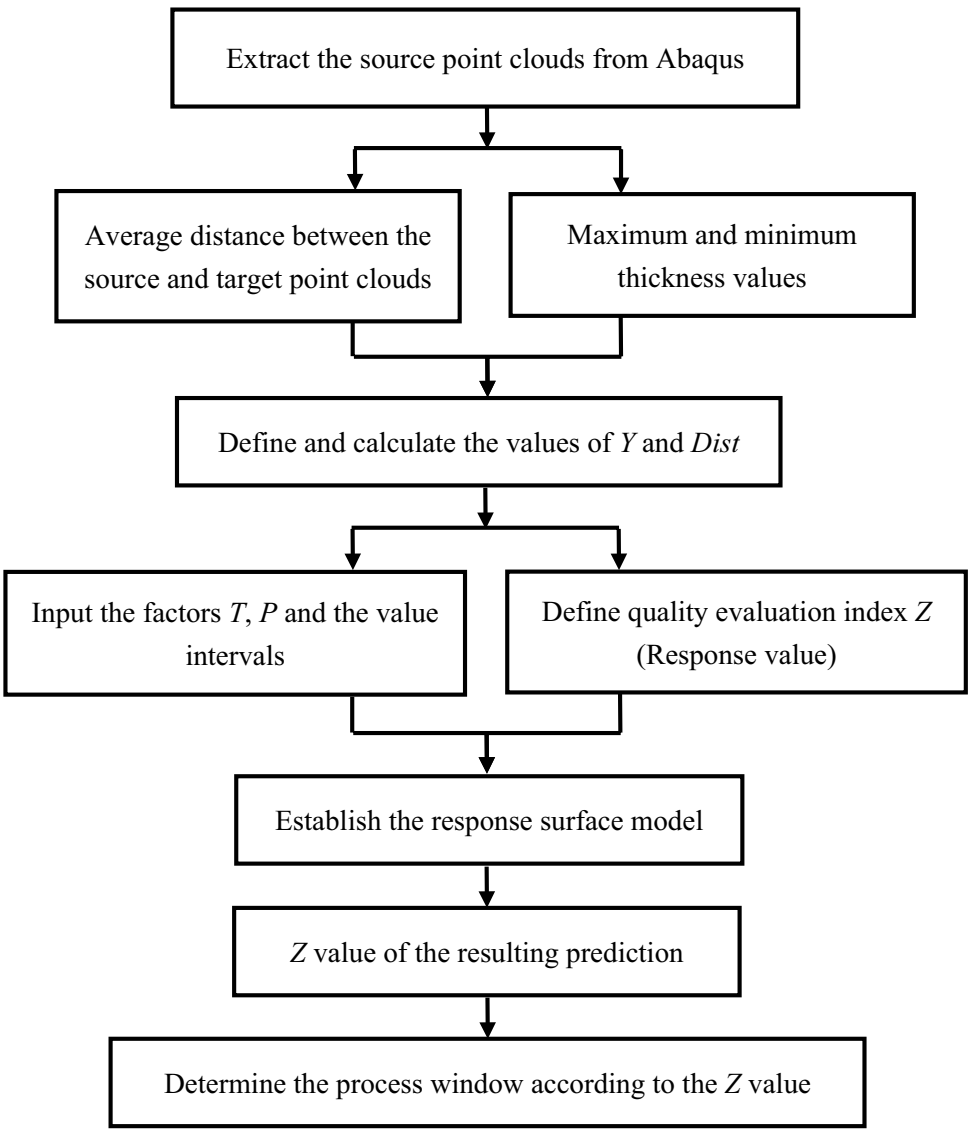

Fig. 10 Flow chart of process window optimization

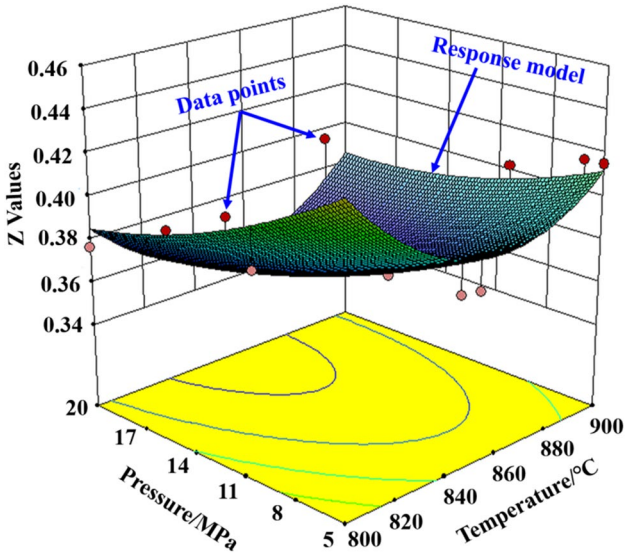

Fig. 11 The prediction chart by response surface analysis

increasing pressure. But it is more sensitive of forming temperature than pressure. The Z value decreased slightly from 0.3781 to 0.3712 with pressure increasing from 5 to 20 MPa at temperature of 850 ℃. The predicted optimal forming temperature and gas pressure were 853 ℃ and 13.6 MPa respectively. However, the length of the formed component was more than 550 mm, which needs large volume high pressure gas. Therefore, a gas pressure of 6 MPa was choose to perform the actual forming. The dimensional accuracy deviation of the component formed at 850 ℃ with gas pressure of 6 MPa was predicted to be 0.42 mm. This value is slightly higher than the actual one. The possible reason is that stress relaxation of titanium alloys at high temperatures reduces spring back. However, it is not considered in the current optimization process.

Determination of weld position during HGPF

The selection of weld position has a significant effect on the HGPF and the improper selection of weld position leads to weld cracks in the deformation process. To determine a reasonable weld position, a simulation of the 2D model with the tube of 5% expansion ratio was used. The equivalent stress in specific positions were calculated as shown in Fig. 12. A rectangular coordinate system (blue dotted line) is established in the horizontal and vertical directions, and the origin of the coordinate is placed in the center of the section (Fig. 12). In position I, the equivalent stress is the largest in the initial stage of the die closing, which may cause the weld cracking. In position II, the stress state of the weld is biaxial tension, and it is easy to cause the crack of the weld during the late HGPF. The weld position in the concave area (the

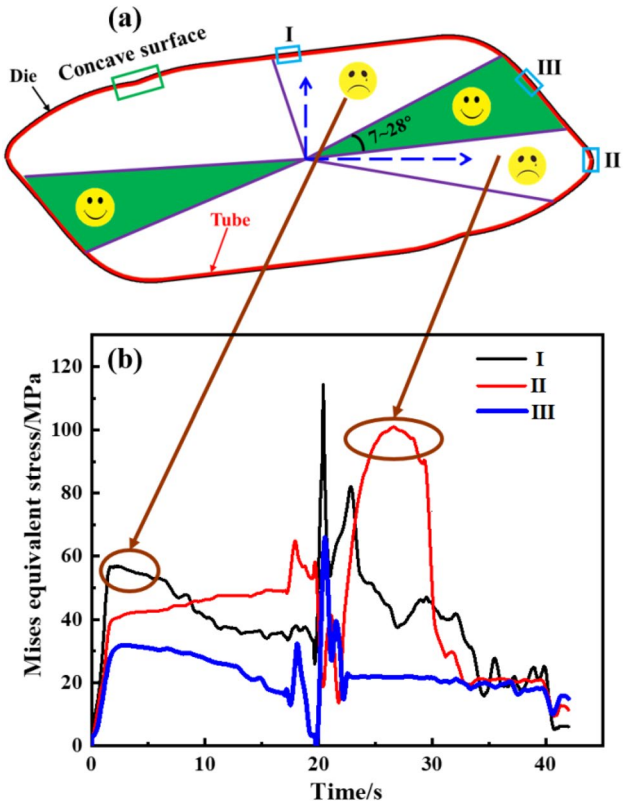

Fig. 12 Characteristic points and equivalent stress of characteristic points. (**a**) the selection region of characteristic points; (**b**) equivalent stress

green rectangular area in Fig. 12a also has the risk of cracking. In position III (7 ~ 28°), the weld is contacted with the die during most of the forming time. The equivalent stress is the smallest in three areas. Therefore, the weld in position III is the reasonable position. As reported in the reference [26], the uniform bulging ratio of the laser-welded titanium alloy tube was close to 43.8% considering shape deviation and uniformity of wall thickness. The maximum strain of the component in this paper is 3% in the weld area, which is much smaller than 43.8%. Therefore, the effect of weld seam on the deformation was neglected.

HGPF of the TC2 alloy irregular profile component

A TC2 component was formed at 850 °C based on the above optimization results, and the specific loading route is shown in Fig. 13. The geometries at different stages are given in the figure.

When the die temperature was elevated to 850 °C, the tube was placed into the die, and then the die was closed for preforming. In the forming process, the gas pressure was increased from 0 to 3 MPa firstly and hold for 15 min, most of the tube area was formed to the ideal position. To improve the forming accuracy of the corner area, the gas pressure was raised from 3 to 6 MPa and hold for 10 min.

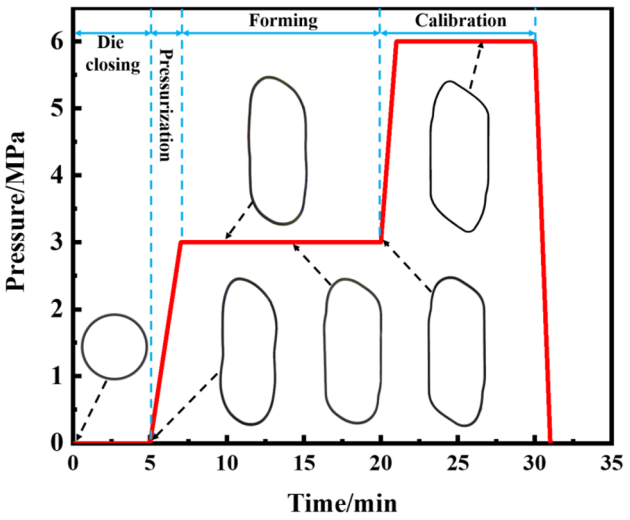

Fig. 13 Specific loading path of the HGPF

Figure 14 shows the TC2 thin-walled irregular profiled component, which was fully formed.

Evaluation of Formed component

To measure the microstructures and properties of the final formed component, the positions of the selected samples are shown in Fig. 15a. Sample (b) and sample (c) are BM and sample (d) is WS. The equivalent strain of the sample (b) was 0.15 and the sample (c) was 0.26. Compared with the initial sheet microstructure in Fig. 0.1 (b), the microstructures of sample (b) and sample (c) varied slightly. Few dynamic recrystallized grains were observed in sample (c). The microstructure of the WS changed a little as shown in Fig. 15d, which was the martensitic decomposing into lath α and β phase due to its unstable at elevated temperature. However, the strain of the WS was relatively small during the forming, so few globalizations was observed after the forming. It could be summarized that the overall microstructures of the final formed component were similar with the initial sheet because of the short forming time during the HGPF.

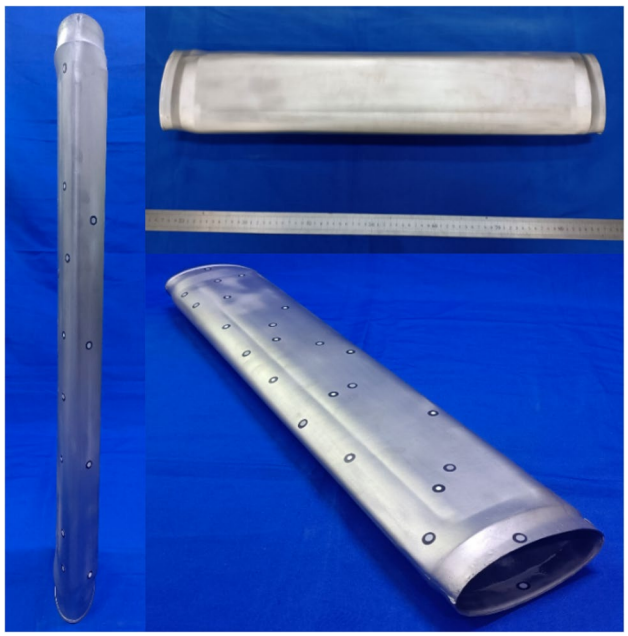

Fig. 14 The final formed TC2 alloy component by HGPF

The room (25 °C) and service temperature (450 °C) properties of the final formed component were evaluated by uniaxial tensile tests as shown in Fig. 16. The properties of BM are almost the same with the initial sheet at both temperatures, but the strength of the weld decreased by 7.05% at 25 °C and 9.54% at 450 °C due to the inevitable decomposition of martensitic at high temperatures. At 450 °C, the average yield stress and tensile stress of BM are 363.1 and 528.6 MPa, respectively. Regarding to the WS, the average yield stress and tensile stress are 423.8 and 538.0 MPa, respectively. The above studies show that the microstructures and properties of the component are basically consistent with those of the initial sheet.

The stress of titanium alloy and steel is dropped significantly after stress relaxation for a certain time at a high temperature [27, 28]. Therefore, the dimensional deviations are less than calculated value obtained above. A 3D Power Scan tester was used to obtain the outer surface of the final formed part. The imaging data was compared with the ideal component by a commercial software of Geomagic Qualify. The dimensional deviation distributions of three specific cross-sections are shown in Fig. 17. The maximum dimensional deviation was about 0.19 mm, indicating the high precision of the part formed by HGPF.

The basic design of HGPF process should consider the forming windows, dimensional accuracy and post-form mechanical properties. According to the hot uniaxial tension tests and microstructure evolutions, the ranges of forming temperature and pressure could be obtained for HGPF. Then the finite element analysis is needed to further optimize the forming process by revealing the effects of forming parameters on the forming defects such as wrinkles, cracks and local serious thinning. The WS has a higher strength than the BM, which could cause non-uniform deformation by localizing deformation in the BM zone. Moreover, the WS has a smaller elongation than the BM, which could cause early fracture failure in the WS during the forming. One should carefully compensate the two possible consequences to design the forming process.

Factors affecting the dimensional accuracy includes the dimension of the forming tools and spring back. The

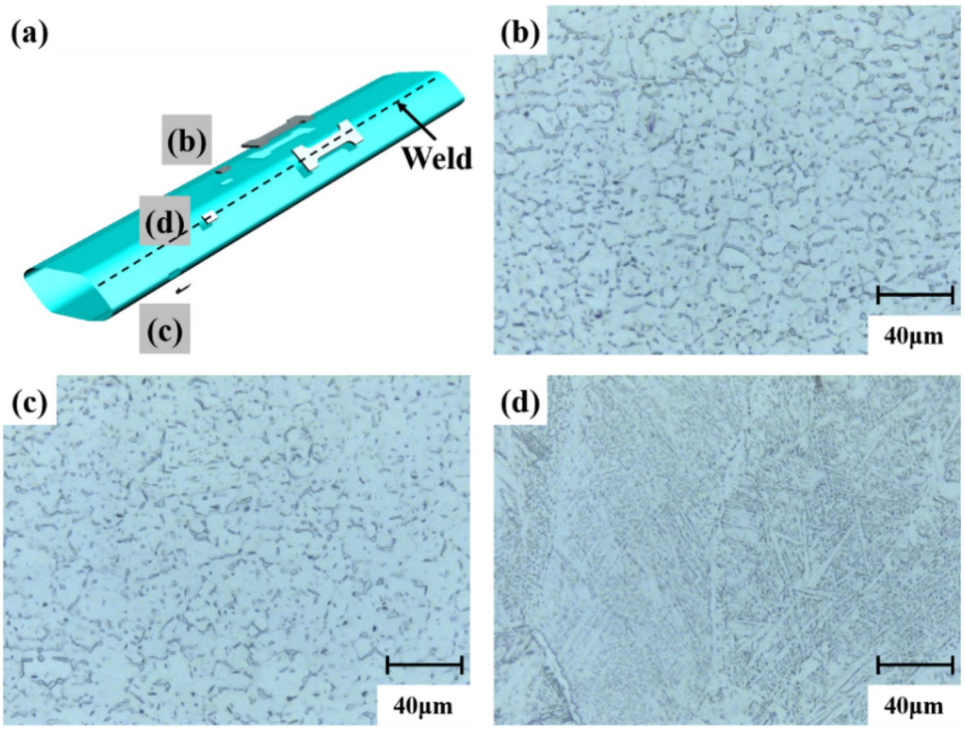

Fig. 15 Microstructure of the final formed part. (**a**) samples positions; (**b**) equivalent strain of 0.15 (BM); (**c**) equivalent strain of 0.26 (BM); (**d**) WS

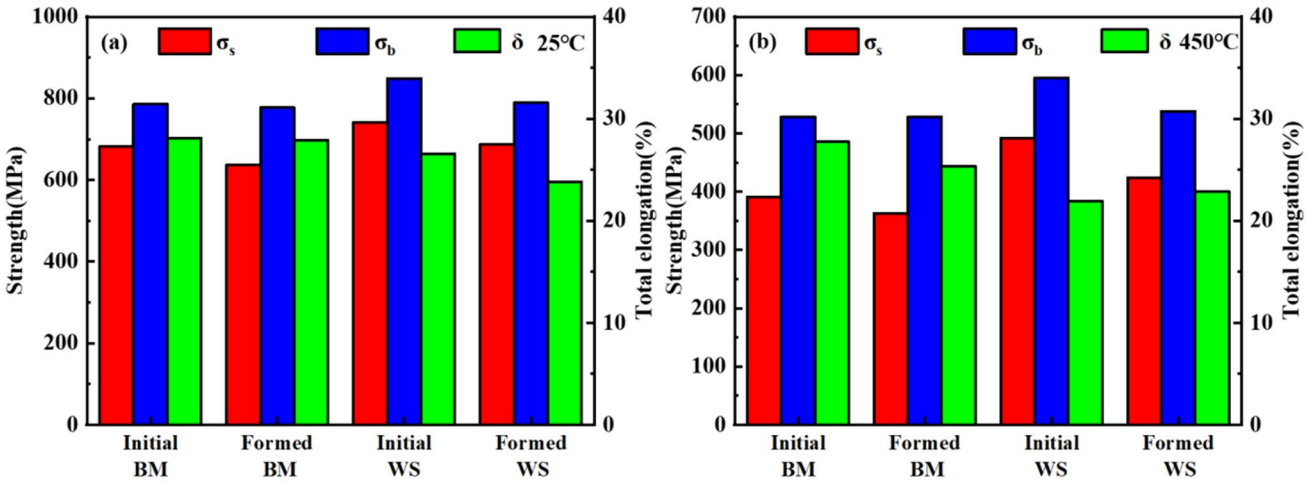

Fig. 16 Mechanical properties of the TC2 alloy before and after HGPF. (**a**) 25 °C and (**b**) 450 °C

materials' thermal expansion coefficients for titanium alloy and forming tools are different, therefore the dimension of the forming tools should be calculated carefully according to the thermal expansion coefficients [29]. The accurate value of thermal expansion coefficient is very important. The spring back could be predicted according to young's modulus and stress relaxation curves. Generally, the spring back could be reduced effectively by increasing the forming temperature. The post-form mechanical properties are mainly controlled by the initial microstructure and deformation parameters including temperature, strain rate, strain and holding time, which should be designed according to the service requirement.

In this paper, both of the microstructure and properties of the BM are close to that of the initial material before and after HGPF. Because of the relatively high forming temperature and long cycle time during the conventional superplastic forming, the post-form properties could decrease compared with the initial material [30]. However, the total heating and forming time of the tube was less than 30 min during the HGPF, therefore almost no strength reduction was observed. Regarding to the dimensional

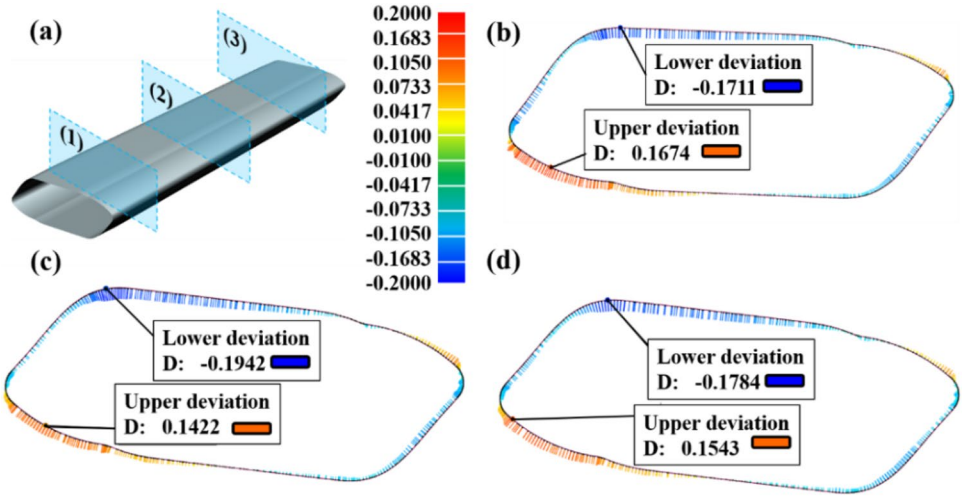

Fig. 17 Dimensional accuracy of the final formed part. (**a**) Measured sections; (**b**) Profile 1; (**c**) Profile 2; (**d**) Profile 3 (unit: mm)

accuracy, components formed by both processes could satisfy the requirements of the service. Therefore, the HGPF process demonstrates the advantages of high efficiency, low energy consumption and excellent mechanical properties compared with the conventional superplastic forming.

Conclusions

In this paper, HGPF process window of a laser-welded TC2 titanium alloy component with irregular profiles was optimized. Hot uniaxial tensile tests, microstructure characterization, finite element simulation and HGPF experiments were studied. The main conclusions are as follows:

1. The microstructure evolution of TC2 titanium alloy is mainly DRX and phase transformation. During the hot deformation of BM with temperature ranging from 750 to 850 °C, DRX is the main factor altering the microstructure evolution, but more phase transformation occurred at 900 °C leading to the formation of secondary α after deformation.
2. The initial size of the tube should be designed carefully to avoid possible wrinkling and severe local thinning. The weld is suggested to be placed in section with the smallest equivalent stress during the HGPF to avoid possible crack.
3. A new method for establishing HGPF window of titanium alloy was proposed. The method of optimizing the process parameters by considering the dimensional accuracy and thickness uniformity was used in the HGPF by RSM. A qualified TC2 titanium alloy component was successfully formed to verify the optimized process window. The mechanical properties of the formed component are similar to that of the initial material and the dimensional deviation of the component only about 0.19 mm could be achieved.

Funding This work was financially supported by the National Natural Science Foundation of China (No. U1937204 and 51401065), Heilongjiang Provincial Natural Science Foundation of China (No. LH2021E058) and China Postdoctoral Science Foundation (2019M661278 and 2021T140153).

Declarations

Conflict of interest The authors declare no competing interests.

References

1. Yuan S (2021) Fundamentals and processes of fluid pressure forming technology for complex thin-walled components. Eng Prc 7:358–366
2. Bell C, Corney J, Zuelli N, Savings D (2020) A state of the art review of hydroforming technology: Its applications, research areas, history, and future in manufacturing. Int J Mater Form 13:789–828
3. Wu F, Xu W, Yang Z, Guo B, Shan D (2018) Study on hot press forming process of large curvilinear generatrix workpiece of Ti55 high-temperature titanium alloy. Metals Basel 8(10):827
4. Trân R, Reuther F, Winter S, Psyk V (2020) Process development for a superplastic hot tube gas forming process of titanium (Ti-3Al-2.5V) hollow profiles. Metals Basel 10:1150
5. Du Z, Zhang K (2021) The superplastic forming/diffusion bonding and mechanical property of TA15 alloy for four-layer hollow structure with squad grid. Int J Mater Form 14:1057–1066
6. Sartkulvanich P, Li D, Crist E, Yu K (2016) Influence of superplastic forming on reduction of yield strength property for Ti-6Al-4V fine grain sheet and Ti-6Al-4V standard. Mater Sci Forum 838–839:171–176
7. Wang K, Wang L, Zheng K, He Z, Politis D, Liu G, Yuan S (2020) High-efficiency forming processes for complex thin-walled

titanium alloys components: state-of-the-art and perspectives. Int J Extrem Manuf 2:032001
8. Wu Y, Liu G, Wang K, Liu Z, Yuan S (2016) Loading path and microstructure study of Ti-3Al-2.5V tubular components within hot gas forming at 800 °C. Int J Adv Manuf Technol 87:1823–1833
9. Dang K, Wang K, Chen W, Liu G (2022) Study on fast gas forming with in-die quenching for titanium alloys and the strengthening mechanisms of the components. J Mater Res Technol 18:3916–3932
10. Wang K, Liu G, Huang K, Politis J, Wang L (2017) Effect of recrystallization on hot deformation mechanism of TA15 titanium alloy under uniaxial tension and biaxial gas bulging conditions. Mater Sci Eng, A 708:149–158
11. Wang K, Liu G, Zhao J, Huang K, Wang L (2018) Experimental and modelling study of an approach to enhance gas bulging formability of TA15 titanium alloy tube based on dynamic recrystallization. J Mater Process Tech 259:387–396
12. Liu G, Wang J, Dang K, Yuan S (2016) Effects of flow stress behaviour, pressure loading path and temperature variation on high-pressure pneumatic forming of Ti-3Al-2.5V tubes. Int J Adv Manuf Technol 85:869–879
13. Liu G, Wu Y, Wang D, Yuan S (2015) Effect of feeding length on deforming behavior of Ti-3Al-2.5 V tubular components prepared by tube gas forming at elevated temperature. Int J Adv Manuf Technol 81:1809–1816
14. Yang J, Wang G, Zhao T, Li Y, Liu Q (2018) Study on the experiment and simulation of titanium alloy bellows via current-assisted forming technology. JOM 70:1118–1123
15. Liu G, Dang K, Wang K, Zhao J (2020) Progress on rapid hot gas forming of titanium alloys: mechanism, modelling, innovations and applications. Procedia Manuf 50:265–270
16. Paul A, Werner M, Trân R, Landgrebe D (2017) Hot metal gas forming of titanium grade 2 bent tubes. AIP Conf Proc 1896:050009
17. Yuan S (2016) Modern hydroforming technology, 2nd edn. National Defense Industry Press, Beijing
18. Aksenov S, Kolesnikov A, Mikhaylovskaya A (2016) Design of a gas forming technology using the material constants obtained by tensile and free bulging testing. J Mater Process Tech 237:88–95
19. Box G, Wilson K (1951) On the experimental attainment of optimum conditions. J R Stat Soc 13(1):1–45
20. Mrabti I, Hakimi A, Touache A, Chamat A (2022) A comparative study of surrogate models for predicting process failures during the sheet metal forming process of advanced high-strength steel. Int J Adv Manuf Technol 121:199–214
21. Jiao X, Wang D, Yang J, Liu Z, Liu G (2019) Microstructure analysis on enhancing mechanical properties at 750 °C and room temperature of Ti-22Al-24Nb-0.5Mo alloy tubes fabricated by hot gas forming. J Alloy Comp 89:639–646
22. Wu R, Liu X, Li M, Chen J (2022) Investigations on the process window for friction stir assisted double-sided incremental forming with synchronous bonding of steel and aluminum alloy sheets. Int J Mater Form 15:3
23. Wang K, Shi C, Zhu S, Wang Y, Shi J, Liu G (2020) Hot gas pressure forming of Ti-55 high temperature titanium alloy tubular component. Materials 13(20):4636
24. Wang K, Jiao Y, Wu X, Qu B, Wang X, Liu G (2021) A novel composited process of solution treatment-hot gas forming and stress relaxation aging for titanium alloys. J Mater Process Tech 288:116904
25. Tang Z, Chen J, Dang K, Liu G, Tao K (2019) Experimental investigation into the electropulsing assisted pulsating gas forming of CP-Ti tubes. J Mater Process Tech 278:116492
26. Wang K, Liu G, Zhao J, Wang J, Yuan S (2016) Formability and microstructure evolution for hot gas forming of laser-welded TA15 titanium alloy tubes. Mater Des 91:269–277
27. Chen Y, Han G, Li S, Li Y, Li Z, Lin Z (2021) Time-dependent spring-back prediction with stress relaxation effect for non-isothermal hot stamping of titanium alloy sheets. Int J Adv Manuf Tech 115:637–653
28. Pérez C, Odenberger E, Schill M, Niklasson F, Åkerfeldt P, Oldenburg M (2021) Spring-back prediction and validation in hot forming of a double-curved component in alloy 718. Int J Mater Form 14:1355–1373
29. Jiang S, Zhang K (2009) Study on controlling thermal expansion coefficient of ZrO2-TiO2 ceramic die for superplastic blow-forming high accuracy Ti–6Al–4V component. Mater Des 30:3904–3907
30. Wang G, Jia H, Gu Y, Liu Q (2018) Research on quick superplastic forming technology of industrial aluminum alloys for rail traffic. Defect Diffus Forum 385:468–473